Available online at www.sciencedirect.com
ScienceDirect
Trans. Nonferrous Met. Soc. China 34(2024) 582−591
Transactions of Nonferrous Metals Society of China
www.tnmsc.cn

Tailoring rejuvenation behavior of Zr-based metallic glass upon deep cryogenic cycling treatment

Wei GUO[1,2,3], Sheng YU[1], Jun DING[3], Shu-lin LÜ[1], Shu-sen WU[1], Mi ZHAO[2,4]

1. State Key Lab of Materials Processing and Die & Mould Technology, School of Materials Science and Engineering, Huazhong University of Science and Technology, Wuhan 430074, China;
2. Research Institute of Huazhong University of Science and Technology in Shenzhen, Shenzhen 518057, China;
3. Center for Alloy Innovation and Design, State Key Laboratory for Mechanical Behavior of Materials, Xi'an Jiaotong University, Xi'an 710049, China;
4. School of Aerospace Engineering, Huazhong University of Science and Technology, Wuhan 430074, China;

Received 30 August 2022; accepted 14 February 2023

Abstract: The rejuvenation behavior of a $Zr_{55}Cu_{30}Ni_5Al_{10}$ (at.%) metallic glass upon deep cryogenic cycling treatment was investigated. The sample was rejuvenated to a larger extent with increasing cyclic number, resulting in a higher enthalpy of relaxation and a lower density. The rejuvenation seems to be saturated after 200 cycles, which may originate from the limited content of free volume in the amorphous structure. The sample subjected to a higher cyclic number showed a lower hardness and better plasticity due to a larger shear transformation zone (STZ) volume. In this case, a lower shear plane formation energy facilitates the generation of multiple shear bands. Furthermore, it is found that the content of free volume has linear relationship with the plastic strain and the STZ volume. The results from molecular dynamics simulation also demonstrates that the atomic volume saturates with a higher degree of rejuvenation at a higher cooling rate of the simulated sample.

Key words: metallic glass; rejuvenation; cryogenic cycling treatment; cyclic number; plasticity

1 Introduction

Bulk metallic glasses (BMGs) have attracted considerable scientific interest for last two decades because of their superior properties, such as high fracture strength and large elastic limit, originating from their unique long-range disordered structures [1−3]. Since they are always fabricated by rapid quenching from liquid state, BMGs always possess a higher configurational potential energy compared with their crystalline counterparts [4]. Consequently, the atomic configurations of the metastable BMGs tend to transform into a lower potential energy state towards crystalline structure, and the so-called structural relaxation occurs [5]. The properties of the relaxed BMGs degrade severely. For example, the relaxation annealing can decrease the fracture toughness of BMGs, and such reduction becomes more remarkable with a higher annealing temperature or a prolonged annealing time. Therefore, relaxation-induced degradation of the crucial properties is one critical issue for the widespread application of BMGs.

Recently, many researches have shown that the energy state of the relaxed BMGs can be recovered again to a more metastable state with a higher potential energy by thermal or mechanical methods, which is called as rejuvenation process [6−8]. For example, SAIDA et al [6] found that reheating the relaxed BMGs to a certain temperature just above their glass transition temperature was effective to

Corresponding author: Mi ZHAO, Tel: +86-27- 87540185, E-mail: zhaomi2018@hust.edu.cn
DOI: 10.1016/S1003-6326(23)66419-2

reset the atomic configuration. In this case, rejuvenation could occur and then the rapid cooling was carried out subsequently, but such treatment is only applicable for relaxed samples since the heating process. MENG et al [7] applied high pressure torsion (HPT) to the relaxed BMGs and found that the glassy state can be rejuvenated by the induced internal stress if the materials were subjected to enough torsion cycles, but the sample size is limited and the rejuvenation is not homogeneously. KETOV et al [9] proposed a novel thermal method to rejuvenate the BMGs by deep cryogenic cycling treatment (DCT), in which the samples are cyclically treated between ambient temperature and 77 K. Assisted by the internal stress generated during cyclically cooling and heating, the improvement in heterogeneity and the free volume in the amorphous structure can contribute to the rejuvenation behavior [10]. However, the essential issues are still unclarified. For example, how to tailor the rejuvenation behavior during DCT feasibly? Is there a limited degree of rejuvenation during DCT? How to link the rejuvenation behavior and mechanical property? In the present study, the rejuvenation behavior is carefully studied for a Zr-based BMG with cyclic numbers varied from 5 to 60, and the microstructures and mechanical properties are investigated in detail.

2 Experimental

Master alloys were prepared by arc-melting high-purity Cu, Zr, Ni and Al metal pieces in a Ti-gettered Ar atmosphere in a water-cooled copper hearth. The alloy was remelted four times to ensure chemical homogeneity. The BMGs were fabricated by casting the master alloy into a copper mold to produce 2 mm-diameter rods. The detailed description of the original developed DCT instrument was described in Ref. [10]. The samples can be cooled and heated between ambient temperature and 108 K cyclically with a good reproducibility in each cycle. The samples were treated with various cyclic numbers of 5, 10, 20 and 60, which are denoted as DCT5, DCT10, DCT20 and DCT60, respectively.

The structure was examined by X-ray diffraction (XRD; Bruker D8 Advance) with Cu K_α radiation and transmission electron microscopy (TEM, JEOL JEM−2100F) with an acceleration voltage of 200 kV. The glass transition temperature (T_g) and the onset crystallization temperature (T_x) were measured by differential scanning calorimeter (DSC, Perkin Elmer Pyris Diamond DSC) in Ar at a heating rate of 20 K/min. The specific heat capacities were measured by comparing tested specimens with a sapphire standard one. The density was measured using an Ar gas pycnometer (AccuPyc II 1340, Micromeritics Co. Ltd.). The specimens used for nano-indentation were cut into small discs with a thickness of 2 mm and mechanically polished to mirror surfaces. Nano-indentation tests (MZT−500, Mitutoyo Co. Ltd.) were performed with the load control mode at a peak load of 100 mN with the loading and unloading rates varied (5, 10 and 20 mN/s). For each sample, at least ten indents were made. The cylindrical compression specimens with a height of 4 mm and a diameter of 2 mm were cut and carefully polished to ensure that their ends were flat and in parallel. Compression tests were performed at a strain rate of $5\times10^{-4}\ s^{-1}$ at room temperature using an Instron 5982 mechanical testing machine. Multiple compression tests using at least four specimens for each thermally treated state were conducted to confirm the reproducibility.

Molecular dynamics (MD) simulations were employed to examine the atomistic details of a variety of glassy states. Analogous to the rejuvenation states induced by the different cyclic number of DCT in the present experiments, our MD simulation sampled a variety of glassy structures by increasing the quenching rate. $Zr_{55}Cu_{30}Al_{15}$, as the protype model of our experimental $Zr_{55}Cu_{30}Al_5Ni_{10}$ BMGs, was prepared by MD simulation using empirical EAM (embedded-atom method) potential. The samples, containing 16000 atoms, were firstly melted at 2500 K for 5 ns under Nose-Hoover thermostat, and then quenched to room temperature with a range of cooling rates between 10^9 and 10^{15} K/s. Periodic boundary conditions were applied in all three directions and the external pressure was maintained around zero during the whole process of cooling. Another 10 ns annealing at room temperature was implemented for each sample.

3 Results and discussion

3.1 Amorphous structure after DCT with various cyclic numbers

Figure 1 shows the XRD patterns of DCT5, DCT10, DCT20 and DCT60, which exhibit similar broad peaks of amorphous structure for all samples without any obvious crystalline peaks. It is indicated that all samples could maintain their amorphous nature after DCT. Figure 2 shows the DSC curves of DCT5, DCT10, DCT20 and DCT60, in which the endothermic glass transition peaks followed with the exothermic crystalline transition ones can be observed. T_g and T_x for all samples are almost equivalent, suggesting that the varied DCT cyclic numbers do not induce great changes in the amorphous structures. The detailed data of T_g and T_x are summarized in Table 1.

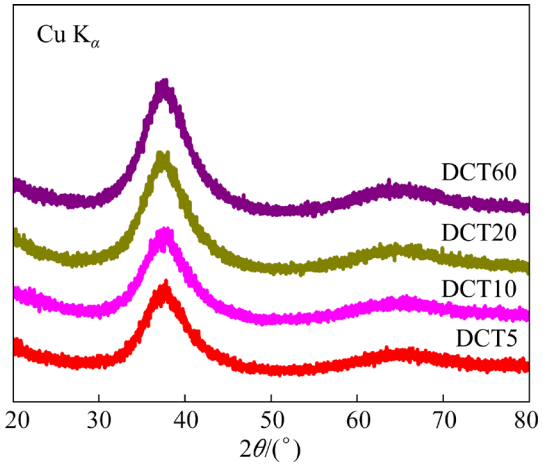

Fig. 1 XRD patterns of DCT5, DCT10, DCT20 and DCT60

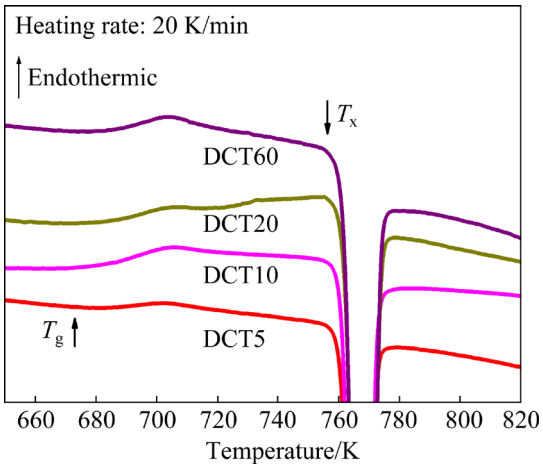

Fig. 2 DSC curves of DCT5, DCT10, DCT20 and DCT60

Table 1 Thermal and physical data for samples in this work

Sample	T_g/K	T_x/K	ΔH_{relax}/(J·g^{-1})	ρ/(g·cm^{-3})	x/%
DCT5	678	759	12.9	6.8204±0.0096	1.45
DCT10	672	761	13.3	6.8181±0.0045	1.52
DCT20	684	762	13.9	6.8173±0.0045	1.54
DCT60	683	760	15.4	6.8102±0.0024	1.75

ρ: density; x: reduced free volume fraction

Figure 3 shows the high-resolution TEM images of DCT5, DCT10, DCT20 and DCT60. The selected area diffraction (SAD) pattern for each sample is inserted. A similar maze characteristic and a halo diffraction pattern of the amorphous structure can be observed for all samples, agreeing well with the XRD results shown in Fig. 1. These results reveal that no crystallization or nano-ordering clusters are formed after DCT with various cyclic numbers.

3.2 Rejuvenation behavior after DCT with various cyclic numbers

The enthalpy of relaxation (ΔH_{relax}) is applied to investigating the relaxation state of an amorphous structure [11,12]. It is given as

$$\Delta H_{relax} = \int_{RT}^{T} \Delta C_p \, dT \quad (1)$$

where $\Delta C_p = C_{p,s} - C_{p,r}$, $C_{p,s}$ and $C_{p,r}$ are the specific heat capacity of the initial glassy state and its relaxed state, respectively. In the present study, we measured the specific heat capacity up to T=723 K (~1.05T_g). Figure 4 shows the specific heat capacity curves of DCT5, DCT10, DCT20 and DCT60 (solid line), as well as their relaxed states (dotted line). Regardless of the similar appearance of curves, the rejuvenation behavior can be detected when the ΔH_{relax} values in Eq. (1) are yielded (listed in Table 1), where an increased ΔH_{relax} can be found with increasing cyclic number. For example, ΔH_{relax} increased by 19.4% (from 12.9 to 15.4 J/g) when the cyclic numbers increase from 5 to 60. This indicates that a more metastable energy state or a more rejuvenated state could be obtained as the cryogenic cycling continues.

Density (ρ) is another important parameter to evaluate the rejuvenation behavior [10]. The densities of DCT5, DCT10, DCT20 and DCT60 are measured and summarized in Table 1. All the

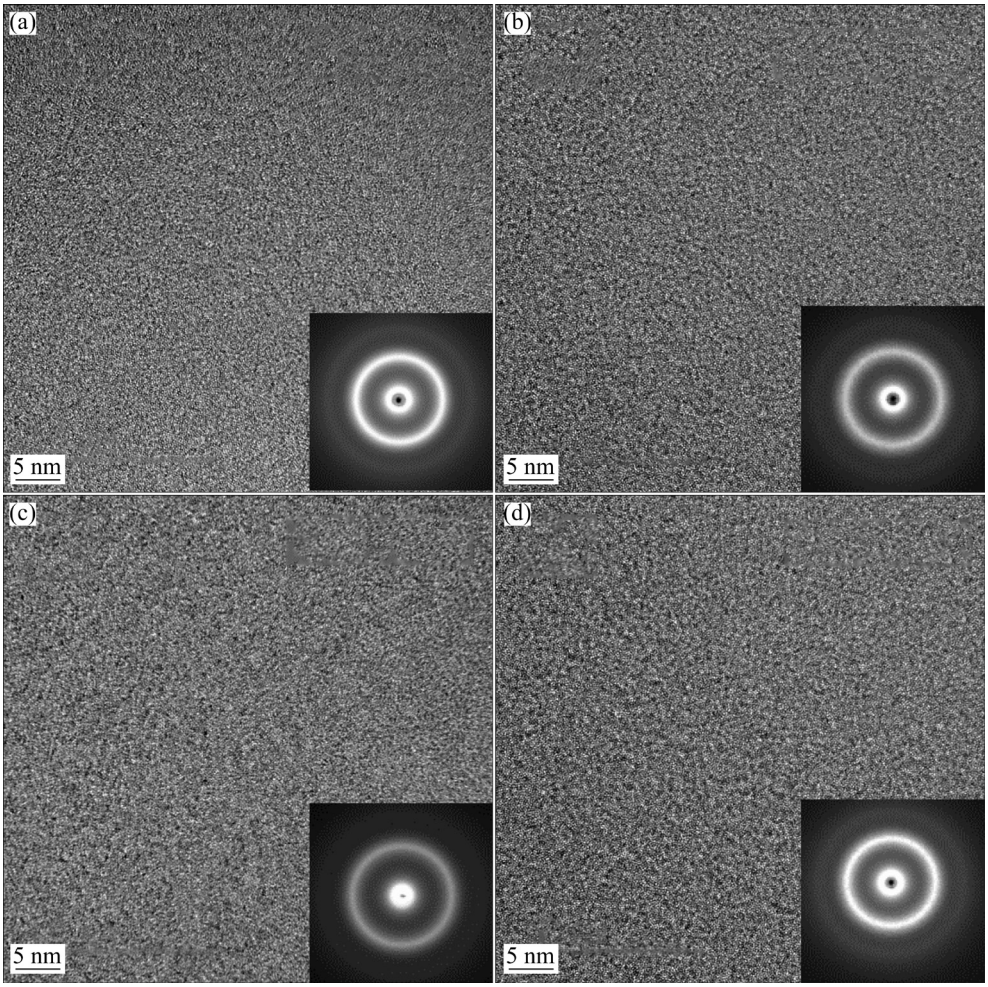

Fig. 3 High-resolution TEM images of DCT5 (a), DCT10 (b), DCT20 (c) and DCT60 (d) (The inset in each figure is the selected area diffraction pattern (SAD) of each sample)

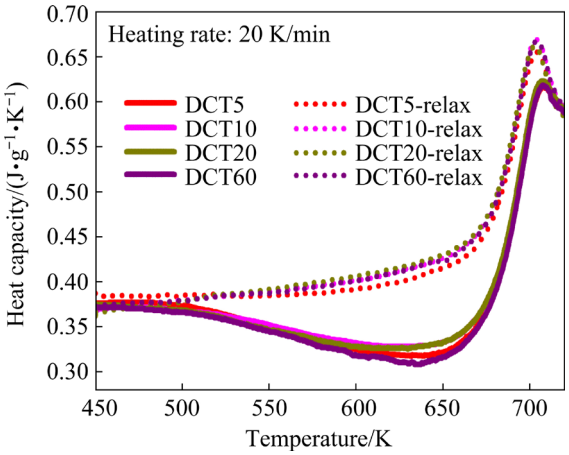

Fig. 4 Specific heat capacity curves of DCT5, DCT10, DCT20 and DCT60

treated specimens possessed lower densities compared with the as-cast one ((6.8243±0.0030) g/cm^3, [10]). The decline in ρ increases as the cyclic number becomes higher. For instance, the density decreased from (6.8204±0.0096) to (6.8102±0.0024) g/cm^3 when the cyclic number increased from 5 to 60. The decrease in density is attributed to the increased free volume upon rejuvenation.

The reduced free volume fraction (x) during relaxation can be calculated as [10,13,14]

$$x=v_f/(\gamma v^*)=2(\rho_c-\rho)/\rho \quad (2)$$

where v_f is the average free volume per atom; γ is the correction term for the free volume overlap; v^* is the critical value of free volume for atomic diffusion; ρ is the density of the sample; ρ_c is the density of a sufficiently crystallized sample, herein measured to be (6.870±0.002) g/cm^3 (annealed at 923 K for 3 h) using the density data in Table 1, the reduced free volumes for all samples were estimated based on Eq. (2) and listed in Table 1. DCT60 possesses the highest x (1.75%) among all

samples. BIAN et al [15] have found that the activation volume during deformation for Zr-based BMG at 77 K is comparable to that near or above T_g. Therefore, the equivalent effects on the atomic structure can be obtained either heating the BMG up to near or above T_g or cooling down to cryogenic temperature. Based on such phenomenon, the atomic structures during DCT are not as rigid as expected and should be adjustable [15].

The above results indicate that increasing the cyclic number can facilitate the rejuvenation process of BMGs. In this case, is there any limit of cyclic number for rejuvenation? Figure 5 shows the values of ΔH_{relax} and x as functions of cyclic number. In order to describe the variation trend, we also plotted the derivative curve of ΔH_{relax} and x in Fig. 5 (see the blue line). It is shown that before 100 cycles, the change of ΔH_{relax} (or x) is obvious, but after that, the rejuvenation seems to saturate, both ΔH_{relax} and x almost maintained unchanged, which indicates that the high cycling number cannot rejuvenate the BMGs effectively. It is reported that the maximum amount of free volume is ~2.5% for a BMG [16]. If the amount exceeds the value, glass transition or phase transformation occurs [16]. Thus, the rejuvenation should reach the maximum limit at a certain cycling number, which can be also proved by the simulation results shown later.

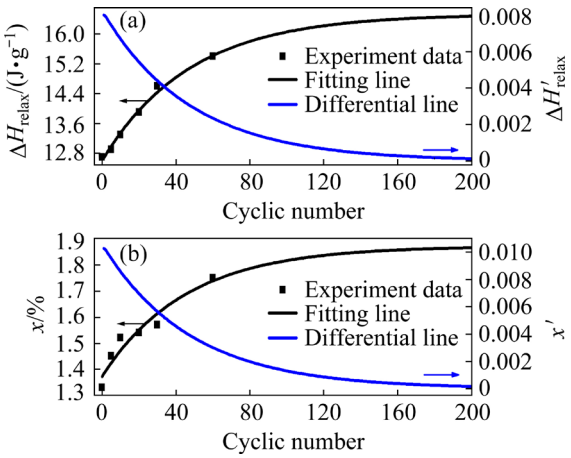

Fig. 5 Fitting of experimental data between cyclic number and ΔH_{relax} (a) and reduced free volume (b) ($\Delta H'_{relax}$ and x' are the derivative of the ΔH_{relax} and x, respectively)

3.3 Mechanical properties after DCT

Figure 6(a) shows the force−depth curves of DCT5, DCT10, DCT20 and DCT60 by nano-indentation. The detailed data of nano-indentation test are summarized in Table 2. Small difference in maximum depth and hardness can be detected for the samples with various cyclic numbers. For example, the hardness (H) of DCT60 ((4.240±0.057) GPa) is lower than that of DCT5 ((4.412±0.038) GPa). A trend can be seen that the higher the cyclic number, the lower the hardness. The decrement in hardness is related with the higher content of induced free volume and consequently a more loosely packed atomic configuration in highly rejuvenated samples [10].

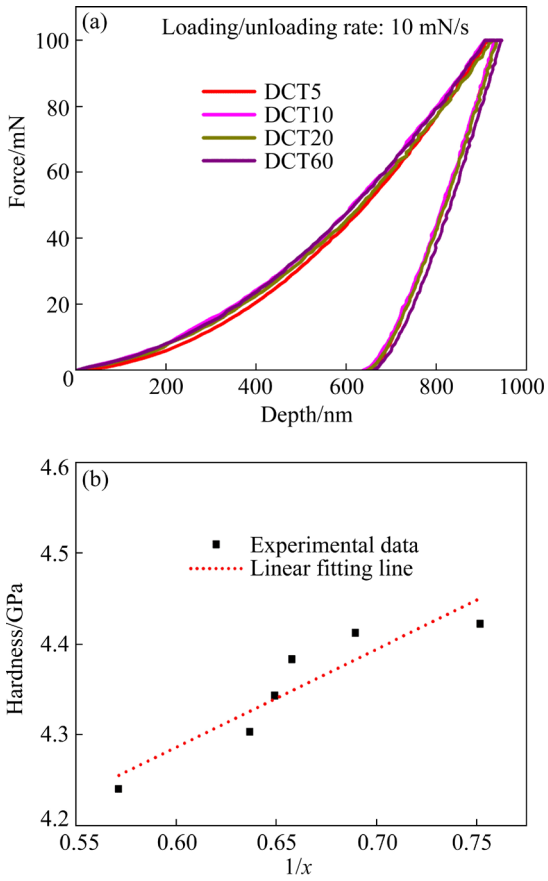

Fig. 6 Force−depth curves of DCT5, DCT10, DCT20 and DCT60 by nano-indentation (a), and relationship between hardness and reduced free volume (b)

It is reported that the quantitative relationship between free volume and hardness (H) can be given as [17]

$$H = AT\sinh^{-1}[B\dot{\gamma}\exp(\frac{\Delta G}{k_B}+\frac{\gamma v^*}{v_f})] \quad (3)$$

where A and B are constants, $\dot{\gamma}$ is the shear strain rate, k_B is the Boltzmann constant, ΔG is the activation barrier energy for defect migration, T is the temperature, and v_f is the average free volume per atom. In the present study, $\dot{\gamma}$, ΔG and T can be

Table 2 Summary of data by nano-indentation and compression

Sample	h_{max}/nm	H_{10}/GPa	E/GPa	σ_f/MPa	σ_y/MPa	ε_f/%	ε_p/%
DCT5	926±5	4.412±0.038	113	2070	1823	8.3	7.2
DCT10	929±5	4.383±0.035	112	2078	1794	9	7.4
DCT20	933±7	4.343±0.052	110	2086	1750	10.9	9.3
DCT60	944±4	4.240±0.057	100	2278	1531	16.3	14.4

h_{max}: maximum depth at loading rate of 10 mN/s; H_{10}: Hardness at loading rate of 10 mN/s; E: Young's modulus; σ_f: Fracture stress; σ_y: yielding stress; ε_f: Fracture strain; ε_p: Plastic strain

approximately estimated unchanged for all samples. Substituting Eq. (2) into Eq. (3), the equation can be rewritten as

$$H=a/x+b \tag{4}$$

where a and b are constants. Figure 6(b) plots the hardness as a function of $1/x$. The experimental data can be well fitted by a linear relation, which agrees well with Eq. (4), indicating that the hardness was influenced by the free volume in the amorphous material.

Figure 7 shows the compressive stress−strain curves of DCT5, DCT10, DCT20 and DCT60. The detailed data of compression test are summarized in Table 2. The sample has a larger plastic strain (ε_p) with an increased cyclic number. It can be seen that ε_p increased from 7.2% for DCT5 to 14.4% for DCT60, with an increase of 100%. However, the yielding strength (σ_y) shows an opposite trend. σ_y of DCT5 is ~1823 MPa and that of DCT60 decreases to ~1531 MPa, resulting in a reduction of 16%. This phenomenon originates from the increased free volume in the rejuvenated amorphous structure with more cryogenic cycles, which gives rise to a more loosely packed region and a lower resistance against shear deformation [18].

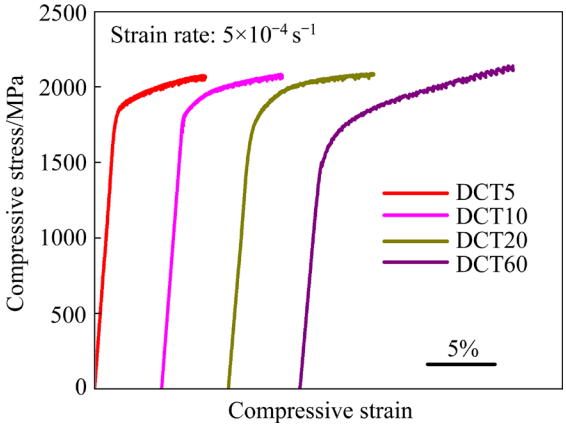

Fig. 7 Compressive stress−strain curves of DCT5, DCT10, DCT20 and DCT60

For BMGs, the stress–strain curves generally exhibit a serrated appearance after yielding and the stress drop is found to be related to the shear band formation [19]. The energy release, ΔE, during a stress drop can be described as

$$\Delta E=\frac{1}{2}\Delta F l=\frac{1}{2}\Delta\sigma\left(\frac{d}{2}\right)^2\pi\varepsilon_e h \tag{5}$$

where ΔF is the load drop; l is the displacement; d and h are the diameter and height of the sample, respectively; $\Delta\sigma$ is the average stress drop [10]; ε_e is the elastic strain. In the present study, $h=2d$. The shear plane area, A, is given by $A=\pi[d/(2\sin\theta)]^2$, where θ is the angle between the shear plane and the loading axis. Therefore, the energy release per shear plane is obtained by

$$\frac{\Delta E}{A}=\varepsilon_e\Delta\sigma d\sin^2\theta \tag{6}$$

Assuming ε_e=0.02, d=2 mm and θ=45°, $\Delta E/A$ can be obtained through Eq. (6). The detailed data are listed in Table 3. It is noted that $\Delta E/A$ decreases with increasing cyclic number, revealing that less energy is required to generate a shear plane for the DCT sample with a higher cyclic number. Therefore, more shear bands can be generated to accommodate the plastic deformation for the highly rejuvenated samples. We plotted the values of $\Delta E/A$ as a function of x in Fig. 8(a). A good linear fitting can be established, which suggests that the change in $\Delta E/A$ was originated from the increased amount of free volume. Besides, the increased free volume also counted for the improved plasticity of BMGs.

The shear transformation zone (STZ) volume, Ω, is obtained to investigate the mechanisms of the plasticization. It can be derived as [20]

$$\Omega=k_BT/(C'Mh) \tag{7}$$

where m is the index of strain-rate sensitivity, and

$$C'=\frac{2R\zeta}{\sqrt{3}}\frac{G_0\gamma_c^2}{\tau_c}\left(1-\frac{\tau_{CT}}{\tau_C}\right)^{1/2},$$

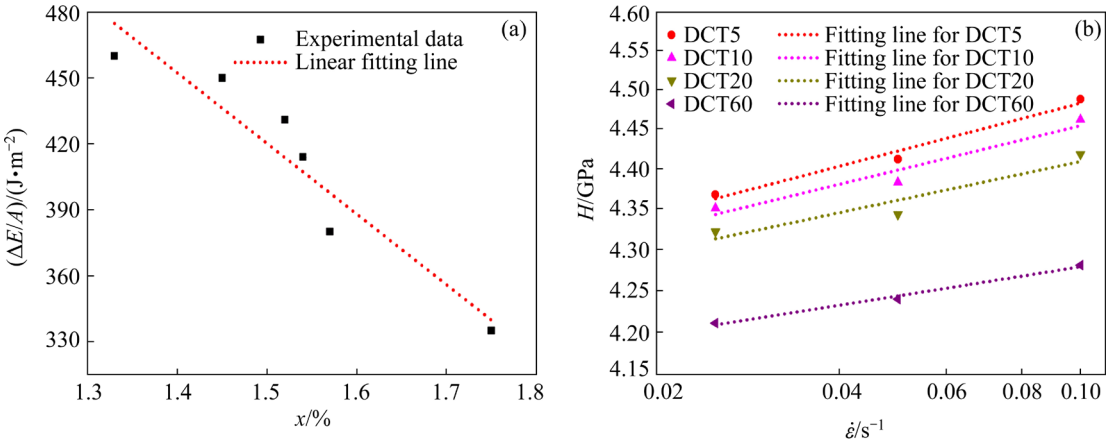

Fig. 8 Relations between shear plane formation energy ($\Delta E/A$) and reduced free volume (x) (a), and determination of strain rate sensitivity, measured by slopes of hardness vs equivalent strain rate (derived from loading rate) curves (b)

Table 3 Summary of data for samples

Alloy	$\Delta\sigma_{ave}$/MPa	$(\Delta E/A)/(J\cdot m^{-2})$	H_5/GPa	H_{20}/GPa	H_{ave}/GPa	m	Ω/nm^3
DCT5	22.5	450	4.368±0.021	4.488±0.034	4.423	0.019	3.617
DCT10	21.55	431	4.351±0.048	4.462±0.027	4.399	0.017	4.065
DCT20	20.68	414	4.322±0.053	4.418±0.047	4.361	0.016	4.356
DCT60	16.77	335	4.211±0.049	4.281±0.054	4.244	0.012	5.969

$\Delta\sigma_{ave}$: Average stress drop after yielding; $\Delta E/A$: Shear plane formation energy; H_5: Hardness at loading rate of 5 mN/s; H_{20}: Hardness at loading rate of 20 mN/s; H_{ave}: Average hardness; m: Equivalent stain-rate sensitivity; Ω: STZ volume

where C' is estimated to be 0.0136 [10]. m can be derived from the equivalent strain rate $\dot{\varepsilon}$ and the hardness value [20]. Here, $\dot{\varepsilon}$ equals to $\dot{P}/(2P)$, where $\dot{P}$ is the loading rate and P is the peak force [20], and the hardness values were averaged from those measured with various loading rates. Thus, by varying the loading rate, 5, 10 and 20 mN/s, $\dot{\varepsilon}$ can be obtained and subsequently m and Ω can be calculated. Figure 8(b) shows the $\dot{\varepsilon}-H$ curves of DCT5, DCT10, DCT20 and DCT60. By fitting the data, m of each sample can be derived. Moreover, assisted with Eq. (7), Ω of each sample is also calculated. The details are summarized in Table 3. It is noted that the more rejuvenated sample possesses a larger Ω.

The plastic deformation in BMGs is accommodated with the shear bands, and the shear bands are initiated by the cooperative shearing of STZs. Once an STZ nucleates, the neighboring one may subsequently generate by the assistance of a local strain field. Thus, a certain number of activated STZs contribute to the formation of a shear band. Therefore, with a larger STZ volume (Ω), less number of STZs are needed to be activated to create a shear band, and consequently a lower formation energy for a shear band ($\Delta E/A$) is required. In other words, a larger Ω promotes the generation of multiple shear bands and helps to improve the plasticity of the BMGs.

Figure 9 shows the relations between reduced free volume (x) and STZ volume (Ω), as well as the relations between free volume and plasticity. Linear relations between x and Ω, and between x and plasticity, can be observed. As stated before, larger excess free volume can be induced by more cryogenic cycles, which should cause a more loosely packed atomic configuration and facilitate the activation of STZs. Here, for the present Zr-based BMG, DCT is proved to be an effective and nondestructive way to rejuvenate and plasticize the sample. The rejuvenation behavior and the mechanical properties can be further tailored by varying the cyclic number.

3.4 Molecular dynamics simulation of various glassy states

Figure 10(a) presents the atomic volume for MD-simulated $Zr_{55}Cu_{30}Al_{15}$ BMGs, prepared with a

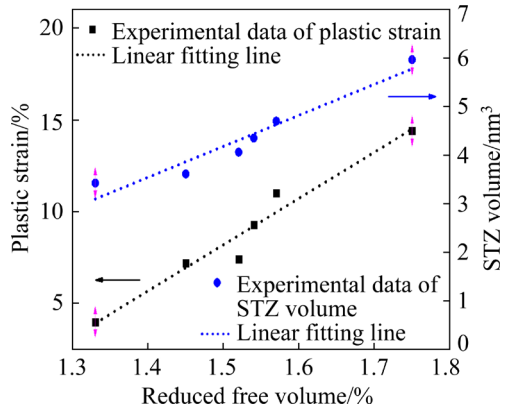

Fig. 9 Relations between plastic strain and STZ volume with reduced free volume

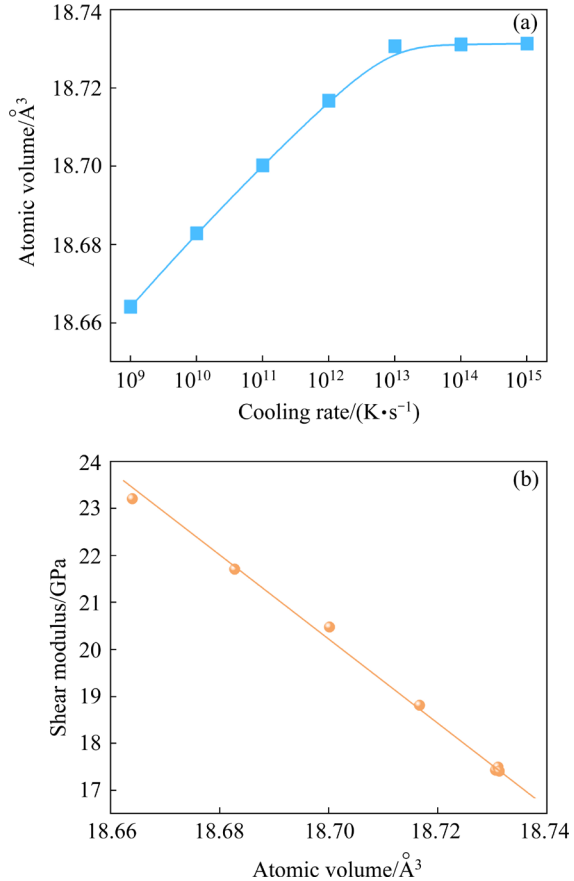

Fig. 10 Atomic volume for MD-simulated $Zr_{55}Cu_{30}Al_{15}$ with various cooling rates, following by room temperature annealing for 10 ns (a), and correlation between atomic volume and shear modulus for MD-simulated $Zr_{55}Cu_{30}Al_{15}$ (b)

variety of cooling rates followed by room-temperature annealing. It is noted that the more rejuvenated samples (i.e., faster cooling rates) generally exhibit larger atomic volumes, which finally reach a plateau at the highly rejuvenated states (i.e., the cooling rates of 10^{13}–10^{15} K/s). Such observation is well consistent with the experimental results (see Fig. 5(b)): the more rejuvenated state corresponds to a more loosely packed atomic structure, as well as a higher fraction of free volume, before reaching the maximum limit of the amount of free volume. In Fig. 10(b), we plot shear modulus and atomic volume for MD-simulated $Zr_{55}Cu_{30}Al_{15}$ BMGs with a variety of glassy states, which exhibited a good linear relationship: the higher atomic volume (or free volume) resulted in the lower shear modulus. This is well consistent with the observation that the hardness of BMGs decreases with increasing content of induced free volume, as demonstrated in Fig. 6.

4 Conclusions

(1) With a higher cyclic number, the samples were rejuvenated to a larger extent with a higher enthalpy of relaxation and a lower density (a larger amount of free volume). The more rejuvenated sample shows a lower hardness and a larger plastic strain, which is originated from the more induced free volume and consequently the more loosely packed atomic configuration.

(2) With more excess free volume, the shear plane formation energy and the STZ volumes become lower and larger, respectively, which will facilitate the formation of multiple shear bands and contribute to the improved plasticity.

(3) The rejuvenation behavior with a high cycling number seems to be saturated, which may be related with the maximum content of free volume in the amorphous structure.

(4) Molecular dynamics simulation shows that the more rejuvenated samples generally exhibit larger atomic volumes, which finally reach a plateau at the highly rejuvenated states. The simulation results agree well with the experimental data.

CRediT authorship contribution statement

Wei GUO: Conceptualization, Methodology, Formal analysis, Resources, Data curation, Writing − Original Draft; **Sheng YU:** Data curation; **Jun DING:** Formal analysis, Investigation; **Shu-lin LÜ:** Investigation; **Shu-sen WU:** Investigation; **Mi ZHAO:** Methodology, Validation, Investigation, Writing − Review & Editing.

Declaration of competing interest

The authors declare that they have no known competing financial interests or personal relationships that could have appeared to influence the work reported in this paper.

Data Availability

The raw/processed data required to reproduce these findings cannot be shared at this time as the data also forms part of an ongoing study.

Acknowledgments

This work was supported by National Natural Science Foundation of China, China (No. 52101138), Natural Science Foundation of Hubei Province, China (No. 2020CFB259), Shenzhen Science and Technology Program, China (No. JCYJ20220530160813032), State Key Lab of Advanced Metals and Materials, China (No. 2020-Z01), State Key Laboratory for Mechanical Behavior of Materials, China (No. 20202205), Guangdong Basic and Applied Basic Research Foundation, China (Nos. 2020A1515110531, 2021A1515111122), State Key Laboratory of Materials Processing and Die & Mold Technology, Huazhong University of Science and Technology, China (No. P2021-021). Jun DING acknowledges support from the National Natural Science Foundation of China (No. 12004294) and National Youth Talents Program, as well as the support by Center for Alloy Innovation and Design (CAID) and HPC platform of Xi'an Jiaotong University. The authors are also grateful to the Analytical and Testing Center of Huazhong University of Science and Technology, China.

References

[1] WANG Fei-long, HAO Qiu-hong, YU Peng-fei, YANG Yu-jing, MA Ming-zhen, ZHANG Xin-yu, LIU Ri-ping. Numerical simulation and experimental verification of large-sized Zr-based bulk metallic glass ring-shaped parts in casting process [J]. Transactions of Nonferrous Metals Society of China, 2022, 32(2): 581−592.

[2] WU Hong, XU Feng, REN Jun-ye, LAN Xiao-dong, YIN Yong, LIANG Lu-xin, SONG Min, LIU Yong, LI Jia, LI Qing-xiang, HUANG Wei-dong. Rate-dependent inhomogeneous creep behavior in metallic glasses [J]. Transactions of Nonferrous Metals Society of China, 2021, 31(6): 1758−1765.

[3] QIAO J C, WANG Q, PELLETIER J M, KATO H, CASALINI R, CRESPO D, PINEDA E, YAO Y, YANG Y. Structural heterogeneities and mechanical behavior of amorphous alloys [J]. Progress in Materials Science, 2019, 104: 250−329.

[4] DEBENEDETTI P G, STILLINGER F H. Supercooled liquids and the glass transition [J]. Nature, 2001, 410 (6825): 259−267.

[5] GUO Wei, YAMADA R, SAIDA J J. Unusual plasticization for structural relaxed bulk metallic glass [J]. Materials Science and Engineering: A, 2017, 699: 81−87.

[6] SAIDA J J, YAMADA R, WAKEDA M. Recovery of less relaxed state in Zr−Al−Ni−Cu bulk metallic glass annealed above glass transition temperature [J]. Applied Physics Letters, 2013, 103(22): 221910.

[7] MENG Fan-qiang, TSUCHIYA K, SEIICHIRO I I, YOKOYAMA Y. Reversible transition of deformation mode by structural rejuvenation and relaxation in bulk metallic glass [J]. Applied Physics Letters, 2012, 101(12): 121914.

[8] GUO Wei, YAMADA R, SAIDA J J, LÜ Shu-lin, WU Shu-sen. Thermal rejuvenation of a heterogeneous metallic glass [J]. Journal of Non-Crystalline Solids, 2018, 498: 8−13.

[9] KETOV S V, SUN Y H, NACHUM S, LU Z, CHECCHI A, BERALDIN A R, BAI H Y, WANG W H, LOUZGUINE-LUZGIN D V, CARPENTER M A, GREER A L. Rejuvenation of metallic glasses by non-affine thermal strain [J]. Nature, 2015, 524(7564): 200−203.

[10] GUO Wei, YAMADA R, SAIDA J J. Rejuvenation and plasticization of metallic glass by deep cryogenic cycling treatment [J]. Intermetallics, 2018, 93: 141−147.

[11] EVENSON Z, BUSCH R. Equilibrium viscosity, enthalpy recovery and free volume relaxation in a $Zr_{44}Ti_{11}Ni_{10}Cu_{10}$-$Be_{25}$ bulk metallic glass [J]. Acta Materialia, 2011, 59(11): 4404−4415.

[12] SAIDA J, YAMADA R, WAKEDA M, OGATA S. Thermal rejuvenation in metallic glasses [J]. Science and Technology of Advanced Materials, 2017, 18(1): 152−162.

[13] HARUYAMA O, INOUE A. Free volume kinetics during sub-Tg structural relaxation of a bulk $Pd_{40}Ni_{40}P_{20}$ metallic glass [J]. Applied Physics Letters, 2006, 88(13): 131906.

[14] SLIPENYUK A, ECKERT J. Correlation between enthalpy change and free volume reduction during structural relaxation of $Zr_{55}Cu_{30}Al_{10}Ni_5$ metallic glass [J]. Scripta Materialia, 2004, 50(1): 39−44.

[15] BIAN X, WANG G, WANG Q, SUN B, HUSSAIN I, ZHAI Q, MATTERN N, BEDNARČÍ J, ECKERT J. Cryogenic-temperature-induced structural transformation of a metallic glass [J]. Materials Research Letters, 2017, 5(4): 284−291.

[16] SPAEPEN F. A microscopic mechanism for steady state inhomogeneous flow in metallic glasses [J]. Acta Metallurgica, 1977, 25(4): 407−415.

[17] LI N, LIU L, CHEN Q, PAN J, CHAN K C. The effect of free volume on the deformation behaviour of a Zr-based metallic glass under nanoindentation [J]. Journal of Physics D: Applied Physics, 2007, 40(19): 6055−6059.

[18] ZHANG M, WANG Y M, LI F X, JIANG S Q, LI M Z, LIU L. Mechanical relaxation-to-rejuvenation transition in a Zr-based bulk metallic glass [J]. Scientific Reports, 2017, 7(1): 625.

[19] DUBACH A, RAGHAVAN R, LÖFFLER J F, MICHLER J,

RAMAMURTY U. Micropillar compression studies on a bulk metallic glass in different structural states [J]. Scripta Materialia, 2009, 60(7): 567−570.

[20] PAN D, INOUE A, SAKURAI T, CHEN M W. Experimental characterization of shear transformation zones for plastic flow of bulk metallic glasses [J]. Proceedings of the National Academy of Sciences of the United States of America, 2008, 105(39): 14769−14772.

深冷循环热处理下锆基金属玻璃的回春行为调控

郭 威[1,2,3]，余 圣[1]，丁 俊[3]，吕书林[1]，吴树森[1]，赵 觅[2,4]

1. 华中科技大学 材料科学与工程学院，材料成形与模具技术全国重点实验室，武汉 430074；
2. 深圳华中科技大学研究院，深圳 518057；
3. 西安交通大学 金属材料强度国家重点实验室 材料创新设计中心，西安 710049；
4. 华中科技大学 航空航天学院，武汉 430074

摘 要：研究 $Zr_{55}Cu_{30}Ni_5Al_{10}$(摩尔分数, %)金属玻璃在深冷循环处理过程中的回春行为。实验发现，随着循环次数的增加，样品的回春程度更高，表现为更高的弛豫焓与更低的密度。回春程度经 200 次循环后逐渐饱和，这可能与非晶结构中有限的自由体积含量有关。同时，高循环次数下的样品硬度更低，塑性更好，这与其剪切转变区体积增大有关。此时，更低的剪切面形成能有利于多重剪切带的形成。此外，还发现自由体积含量与样品塑性应变及剪切转变区体积呈线性关系。分子动力学模拟结果还表明，在高冷速下回春程度高的样品会发生原子体积的饱和。

关键词：金属玻璃；回春；深冷循环热处理；循环次数；塑性

(Edited by Xiang-qun LI)